Chemical Engineering Journal Advances 10 (2022) 100282

Contents lists available at ScienceDirect

Chemical Engineering Journal Advances

journal homepage: www.sciencedirect.com/journal/chemical-engineering-journal-advances

Revealing the adsorption mechanism of copper on hemp-based materials through EDX, nano-CT, XPS, FTIR, Raman, and XANES characterization techniques

Chiara Mongioví [a], Grégorio Crini [a,*], Xavier Gabrion [b], Vincent Placet [b], Virginie Blondeau-Patissier [c], Anna Krystianiak [d], Sylvie Durand [e], Johnny Beaugrand [e], Angelina Dorlando [e], Camille Rivard [f,g], Landrot Gautier [g], Ana Rita Lado Ribeiro [h], Dario Lacalamita [a], Bernard Martel [i], Jean-Noël Staelens [i], Aleksandra Ivanovska [j], Mirjana Kostić [k], Olivier Heintz [d], Corina Bradu [l], Marina Raschetti [b], Nadia Morin-Crini [a]

[a] Laboratoire Chrono-environnement, UMR 6249, UFR Sciences et Techniques, Université Bourgogne Franche-Comté, 16 route de Gray, 25000 Besançon, France
[b] FEMTO-ST, Department of Applied Mechanics, Université Bourgogne Franche-Comté, 25000 Besançon, France
[c] FEMTO-ST, Département Temps-Fréquence, UMR CNRS 6174, Université Bourgogne Franche-Comté, 26 chemin de l'épitaphe, 25030 Besançon, France
[d] Laboratoire Interdisciplinaire Carnot de Bourgogne, UMR 6303 CNRS, Université Bourgogne Franche-Comté, 9 avenue Alain Savary, BP 47870, 21078 Dijon cedex, France
[e] BIA, UR1268, INRAE, 44316 Nantes, France
[f] TRANSFORM, UAR 1008, INRAE, Imp. Yvette Cauchois, 44300 Nantes, France
[g] Synchrotron SOLEIL, L'Orme des Merisiers, 91190 Saint-Aubin, France
[h] Laboratory of Separation and Reaction Engineering - Laboratory of Catalysis and Materials (LSRE-LCM), Faculdade de Engenharia, Universidade do Porto, Rua Dr. Roberto Frias s/n, 4200-465 Porto, Portugal
[i] Univ. Lille, CNRS, INRAE, ENSCL UMR 8207, UMET – Unité Matériaux et Transformations, Lille, France
[j] Innovation Center of the Faculty of Technology and Metallurgy, University of Belgrade, Karnegijeva 4, 11000 Belgrade, Serbia
[k] Department of Textile Engineering, Faculty of Technology and Metallurgy, University of Belgrade, Karnegijeva 4, 11000 Belgrade, Serbia
[l] University of Bucharest, Department of Systems Ecology and Sustainability, PROTMED Research Centre, Spl. Independentei 91-95, 050095 Bucharest, Romania

ARTICLE INFO

Keywords:
Hemp shives
Copper
Adsorption
Mechanism

ABSTRACT

Hemp-based materials have been recently proposed as adsorbents for metals present in aqueous solutions using adsorption-oriented processes. This study aims to reveal the adsorption mechanism of materials prepared from hemp shives as co-products of the hemp industry, namely sodium carbonate-activated (SHI-C) and polycarboxylic agent-grafted (SHI-BTCA) hemp shives. The interactions between copper and two hemp-based materials were characterized by different microscopic and spectroscopic techniques such as energy-disperse X-ray (EDX) spectroscopy, computed nano-tomography (nano-CT), X-ray photoelectron spectroscopy (XPS), Fourier-transform infrared (FTIR) spectroscopy, Raman spectroscopy, and X-ray absorption near-edge structure (XANES) spectroscopy. The results showed remarkable different mechanisms for copper adsorption onto the SHI-C and SHI-BTCA hemp shives. Namely, copper surface adsorption and diffusion in the structure of the SHI-C material were predominant, whereas the adsorption of copper onto SHI-BTCA was due to a chemisorption phenomenon and ion-exchange involving the adsorbent carboxylate groups. The combination of the above-mentioned complementary microscopic and spectroscopic techniques allowed us to characterize and distinguish the type of interactions involved in the liquid-solid adsorption phenomena.

1. Introduction

Industrial hemp is an annual crop grown for its seed and fibers [1,2]. The three main global producers of hemp are China, Europe, and North America. Hemp is found in countless daily products: foods (flour, oils, butter, energy bars, chocolate, yogurts, ice cream, cheese), beverages

* Corresponding author: ORCID: 0000-0003-2540-6851
E-mail address: gregorio.crini@univ-fcomte.fr (G. Crini).

https://doi.org/10.1016/j.ceja.2022.100282
Received 7 February 2022; Received in revised form 28 February 2022; Accepted 1 March 2022
Available online 4 March 2022

(milk, infusions, cocktails, brewed beers, and wines), cosmetics, and personal care products (soaps, shampoos, creams, hand sanitizer, skin moisturizer, hair care), textiles (clothing, fabrics, shoes, mats, ropes), papers and cardboard (cigarette paper, toilet paper), jewelry and fashion, leisure products (fishing, sports), animal feed, animal litter, mulching and horticulture, detergents, biofuel, building materials, insulation, composites (plastics, automotive), etc [3–10]. Hemp is also the object of numerous fundamental studies for innovative potential applications in biopesticides, biotechnology, pharmacy and medicine, paints, energy production, and wastewater treatment [11].

Hemp shives, as valuable co-products produced during the process of extracting fiber from hemp straw, are constituted from the xylem tissue of the stem. Long considered as a by-product of the industry, used for plant mulch or animal bedding (cats, horses), hemp shives are now used for house insulation, energy, and fuel production [7-10,12,13]. There is also an interest in using these co-products as adsorbent materials to complex environmental pollutants since this resource is abundant, cheap, and easily burned. The last one is interesting in the context of recovery of adsorbed metals and their revalorization for example. Moreover, these materials have a highly reactive lignocellulosic macromolecular structure capable of interacting with other substances [3,5,8]. Finally, the industry also needs to find new outlets because the volume of shives produced annually is constantly increasing [11]. Recently, hemp fibers have been studied as adsorbent for metal removal [14–25] and for the preparation of activated carbons for similar applications [26–28]. However, work on hemp in shives/hurds form for environmental applications is rare [11,22,25]. Furthermore, the identification of interactions involved in liquid-solid adsorption phenomena is often carried out using empirical mathematical models that allow the modeling of experimental results and the drawing of conclusions from the assumptions of these models. Another approach is to couple different microscopic and spectroscopic techniques to obtain information on these mechanisms [29,30].

This study is part of the European research project FINEAU which brings together academics and industrialists focused on the potential use of hemp shives to recover metals from industrial effluents aiming their valorization [31]. Two types of materials were targeted in this study by comparing shives washed with water (SHI-W) with those chemically modified using polycarboxylic agent (1,2,3,4-butanetetracarboxylic acid, BTCA, SHI-BTCA sample), and with shives washed with water and activated with sodium carbonate (SHI-C sample). The last one was the most efficient biosorbent of copper in our previous study among investigated raw shives and those treated with H_2O, H_3PO_4, or KOH [31]. The chemical treatment with Na_2CO_3 was carried out on a laboratory scale by copying the process already used by one of the industrialists of the project on other cellulosic materials. The grafting with BTCA was carried out in the laboratory using a previously published procedure [32]. The objective of these two modifications is to purify and increase the capacity of raw shives towards metals, while presenting high selectivity and performances independently of the pH and ionic strength representing two important issues for wastewater from the surface treatment industry. Recently, Mongioví et al [30,31] reported that in the context of copper recovery by SHI-C and SHI-BTCA samples, these two materials had similar high adsorption capacities and fast adsorption kinetics, while their adsorption behaviors were very different. For example, the pH of the solution after copper adsorption onto the SHI-BTCA sample increased significantly, while that of the SHI-C sample varied much less, suggesting different interactions between these shives samples and the adsorbed copper. In addition, the amounts of sodium released into the solutions after an exchange with metal ions increased strongly in the case of the SHI-BTCA sample due to the presence of COONa groups in this material, also confirming different adsorption mechanisms [30].

This study has two objectives: the first is to characterize the surface state of the materials before and after copper adsorption and the second is to assess the interactions between the materials and the metal ions involved in the adsorption process using microscopic and spectroscopic tools, namely computed nano-tomography (nano-CT), energy-disperse X-ray (EDX) spectroscopy, X-ray photoelectron spectroscopy (XPS), Fourier-transform infrared (FTIR) spectroscopy, Raman spectroscopy, and X-ray absorption near-edge structure (XANES) spectroscopy.

2. Experimental section and sample characterization

2.1. Raw hemp shives

The raw hemp shives, abbreviated SHI-R, came from the operation of fiber extraction from the hemp stalk used to recover the hemp fibers. They were supplied by an agricultural cooperative (Eurochanvre, Arcles-Gray, France). They are constituted by parallelepiped particles whose length varies from 5 up to 25 mm, with a density of 100 kg/m^3, thermal conductivity of 0.05 W/mK, and an average price of 0.90 euros/kg, being commercialized for plant and animal mulching, and insulation.

2.2. Modification of hemp shives

Three different treatments were applied to SHI-R samples. A water washing (SHI-W), an activation using sodium carbonate (SHI-C), and a grafting reaction using 1,2,3,4-butanetetracarboxylic acid (SHI-BTCA) were carried out to study their role in the performance of samples which were further used as adsorbents for copper presents in aqueous solution [30,32].

To prepare SHI-W, SHI-R samples were simply washed with water for 2 days at room temperature (22 ± 1°C). After that, they were filtered and dried in an oven at 80°C until a constant mass was obtained.

The SHI-C shives were prepared by treating SHI-W samples in 1 M Na_2CO_3 for 4 h at 40°C. Thereafter, the samples were washed extensively with water until a neutral pH was obtained and dried in an oven at 80°C until a constant mass was obtained.

To obtain SHI-BTCA, SHI-W samples were pre-treated with 1 M NaOH for 3 days at ambient temperature under mechanical stirring. The shives suspension was then filtered on a filtering funnel and thoroughly washed with distilled water until the water was colorless. After drying at 60°C in a ventilated oven (Memmert, France) for 15 h, the samples were immersed in an aqueous solution containing 100 g/L of BTCA and 30 g/L of $NaPO_2H_2$ (Aldrich, France) for 15 h at ambient temperature under mechanical stirring. After draining, shives were spread on the bottom of a glass crystallizer put in a ventilated oven at 160°C for 90 min. They were suspended in distilled water overnight under stirring, filtered, thoroughly washed with distilled water, and dried in a ventilated oven at 60°C for 15 h. The shives were finally activated by converting the acidic form of carboxylic groups into their basic carboxylate form by immersing materials in a $NaHCO_3$ solution (20 g/L) under mechanical stirring for 24 h. SHI-BTCA samples were filtered, washed with distilled water until neutral pH was reached, and dried in a ventilated oven at 60°C for 15 h [32].

2.3. Reagents

Copper sulfate salt was purchased from Sigma-Aldrich (France) and used as received. Appropriate weights of copper sulfate were dissolved in water to obtain a stock solution containing 300 mgCu/L (initial pH of the metal solution = 4.5 ± 0.1). Solutions having lower copper concentrations were obtained by dilution. All solutions were analyzed by Inductively Coupled Plasma-Atomic Emission Spectrometry (ICP-AES, ThermoFisher, iCAP 6500 radial model, Courtaboeuf, France) following a standard protocol prior to each experiment.

2.4. Adsorption experiments

The effect of initial copper concentration on its removal by shives was studied by batch experiments using the following procedure: 2 g of

shives were stirred with 100 mL of an aqueous solution (pH 5 ± 0.1) at known concentrations of copper in a tightly closed flask on a thermostatic mechanical shaker operating at 250 rpm for 2 h at room temperature (22 ± 1°C). The shives were then withdrawn and each solution was analyzed using ICP-AES. The adsorption performance of shives was calculated and expressed as a percentage of removed copper. At the end of each experiment, a slight pH increase between 0.5 and 0.8 units and between 0.8 and 1.5 pH units occurred for SHI-C and SHI-BTCA, respectively (no variation was observed for the SHI-W sample). Each experiment was repeated five times under identical conditions, showing reproducibility.

2.5. Chemical composition and ion-exchange capacity

The determination of the chemical composition of hemp shives is detailed elsewhere [30,31]. Briefly, the hemp shives' non-cellulosic components were removed as follows: i) water-soluble components (extraction with boiling water); ii) fats and waxes (Soxhlet extraction with dichloromethane); iii) pectins (treatment with ammonium oxalate at boiling temperature); iv) lignin (treatment with sodium chlorite at boiling temperature); and v) hemicelluloses (treatment with sodium hydroxide at room temperature). After removal of the non-cellulosic components, α-cellulose remained as a solid residue. For each sample, the chemical composition was determined in duplicate. The ion-exchange capacity of the three samples was determined by pH-metric titration previously reported by Loiacono et al [32].

2.6. Computed nano-tomography analysis

The nano-CT investigation was performed with an RX Solutions EasyTom 160 equipped with an X-ray source Hamamatsu Open Type Microfocus L10711 (RX Solution, Chavanod, France). The X-ray transmission images were acquired using a detector 2530DX of 2176 × 1792 pixels^2. The following conditions were used: tube voltage of 60 keV, tube current of 86 μA, exposure time at 6 images per second with an average frame of 6 images, and 1440 projections collected for each sample resulting in a time of 30 min per tomograph. The entire volume was reconstructed at a full resolution with a voxel size of 1.4 μm corresponding to a field of view of 2.8 × 2.5 mm^2, using filtered back-projection. The data analysis was processed using VG StudioMax software. For shives exposed to copper adsorption, a segmentation was realized using visually interpreted thresholds and prior knowledge. Indeed, the grey level depends on the density of the material. Three distinct peaks attributed to air, cell wall material, and copper, were found in the multimodal image histogram. Thresholds were then positioned between the respective peaks and each material family was then represented by a color: air in black, cell walls in grey, and copper in red.

2.7. Energy-disperse X-ray spectroscopy

The surfaces of samples were examined on a scanning electron microscope (Apreo, ThermoFisher Scientific, Courtaboeuf, France) with a tungsten filament voltage from 15 keV to 20 keV and low-vacuum conditions. Elemental analysis of the sample surfaces was then performed using the Thermo NORAN system for EDX spectroscopy and the electron beam excitation (ThermoFisher Scientific, The Netherlands). EDX spectra recorded at these specific surface locations were then analyzed to evaluate the influence of treatments and copper exposure on the elemental composition.

2.8. Fourier-transform infrared spectroscopy

Shives samples were immersed for 8 min in N_2 liquid (Cryo-Grinder™) and FTIR spectra were recorded from KBr pellets containing 2 mg of sample and 120 mg of KBr. The spectra were collected in transmission mode between 4000 and 400 cm^{-1} at 2 cm^{-1} resolution with an IS50 spectrometer (ThermoFisher Scientific, Courtaboeuf, France). The infrared spectra resulted from 200 co-added scans using the OMNIC 9.2.41 software. All spectra in the 2000-700 cm^{-1} region were baseline-corrected and unit vector normalized using the OPUS 7.5 software (Bruker Optics, France). Mean spectra were calculated with The Unscrambler 10.1 software (CAMO, Oslo).

2.9. Raman spectroscopy

Samples of shives were observed on the aluminum slide and Raman spectra were recorded using a confocal Raman microspectrometer InVia (Renishaw, Marne la Vallée, France). Confocal Raman microscopy is a sensitive surface technique with a spatial resolution in the order of 250-500 nm. A 785 nm laser excitation from 100 to 1 mW according to the sensitivity of the sample to burn with a grating of 1200 grooves/mm was used. The spectra were collected between 200 and 2000 cm^{-1} at 1 cm^{-1} resolution with an X50 objective and a pinhole of 65 μm. Data acquisition and processing, in order to remove spikes and baseline correction, were performed with Wire 4.2 software. The smoothing process, vectorial normalization, and mean spectra were processed with The Unscrambler 10.1 software (CAMO, Oslo, Norway).

2.10. X-ray photoelectron spectroscopy

Chemical surface analyses of the samples were studied on a Versaprobe 5000 spectrometer (ULVAC-PHI, Inc.) equipped with a monochromatized and a focalized Al Kα X-ray source (1486.6 eV). For each sample, survey spectra, as well as high-resolution core-level windows of carbon 1s, oxygen 1s, and copper 2p levels, were acquired over a spot size of 200 μm and a pass energy of 187.5 eV for spectra and 58.7 eV for windows. LMM Auger transition for copper was monitored to make the difference between Cu(I) and Cu(0) [33,34]. Data processing was done using Casa XPS software and energy calibration was done on CC/CH bonds (1s level at 284.8 eV). The quantification of metallic atoms (atomic concentrations in %) before and after adsorption was obtained from the measurement of the corresponding peak area and the use of relative sensitivity factors (RSF), specific of the spectrometer and furnished by the manufacturer. To approach the effective atomic surface concentrations, all the atoms detected on the surface were taken into account. For one atom, the signal obtained can be decomposed into different contributions relative to various chemical species. The calculation of the respective contribution of each peak area will lead to the knowledge of the relative proportion of each chemical form for a given atom.

2.11. X-ray absorption near-edge structure spectroscopy

XANES measurements were performed to determine the Cu speciation. Cu K-edge XANES spectra were recorded on the SAMBA beamline at the SOLEIL synchrotron (Saint-Aubin, France). The Si (220) monochromator was calibrated to 8979 eV at the first inflection point of the Cu foil XANES spectrum. Powders of shives samples SHI-C and SHI-BTCA containing copper (i.e., samples SHI-CCu, SHI-BTACCu), and $CuSO_4$,$5H_2O$ (Sigma-Aldrich) were diluted into cellulose and pressed into 6 mm pellets for optimal transmission analysis. The pellets were sealed in Kapton tape, placed on a sample rod, quenched in liquid nitrogen, and then introduced into a He cryostat (T = 20 K). One continuous XANES scan was recorded in transmission mode using an ionization chamber, in the 8900-9193 eV energy range with a monochromator velocity of 10 eV/s and an integration time of 0.025 s/point. The obtained scans were then normalized and background-subtracted using the Athena featured in the Demeter software package [35].

3. Results and discussion

3.1. Characterization of the SHI-W, SHI-C, and SHI-BTCA samples before use as adsorbents

The results presented in Table 1 showed changes in the chemical composition of the samples after activation and grafting treatments. The chemical composition data for SHI-W and SHI-C samples can be directly compared since the latter material was obtained from SHI-W by alkaline treatment. As expected, after the treatment with Na_2CO_3 (SHI-C sample), water-soluble components, fats, and waxes were removed, while an increase in the percentage of cellulose was observed. Alkaline treatment also resulted in the reduction of the hemicellulose content, while the content of lignin did not vary, suggesting that it is highly resistant to this chemical reaction [31]. Such behavior was also observed for alkaline treated jute [36]. It is difficult to compare the chemical composition of SHI-W and SHI-C with that of the SHI-BTCA sample since its chemical composition is very different from those of the mentioned samples. Nevertheless, the ion exchange capacity data revealed that the amount of carboxyl groups present in the SHI-BTCA sample (1.50 meq/g) was much higher than in the case of the other two samples (0.13 and 0.31 meq/g for SHI-W and SHI-C, respectively), confirming the grafting reaction of BTCA molecules on the cellulosic support by esterification reaction [32].

3.2. Adsorption data

SHI-W, SHI-C, and SHI-BTCA samples having different chemical compositions and in-exchange capacities were used as adsorbents for cupric cations present in copper(II) sulfate solutions using an adsorption-oriented process. Fig. 1. illustrates the impact of the initial copper concentration on the performance of the three shives samples to remove copper from the aqueous solution. These data clearly demonstrated that SHI-C and SHI-BTCA were more efficient for adsorbing copper than SHI-W, which is in agreement with recently published data [30]. In terms of purification efficiency, the order obtained is as follows: SHI-C ~ SHI-BTCA >> SHI-W, which is especially pronounced for concentrations above 25 mg/L (Fig. 1).

By increasing the copper initial concentration from 25 up to 300 mg/L, the efficiency of the SHI-W sample decreased sharply, i.e., the percentage of removed copper was reduced from 90 down to 20 %. If we express the results in concentration, a dosage of 1 g of material removed 1.48 and 3.23 mg of copper from the 2.5 and 30 mg present in 100 mL of solution, respectively. Curiously, besides their different chemical compositions, the SHI-C and SHI-BTCA samples have similar performances whatever the initial copper concentration and their efficiencies were less influenced by the concentration increase. In addition, up to 100 mg/L, their efficiencies were remarkable since the removal was complete (~100%), with a slight and similar decrease in their performances when initial copper concentrations were higher than 100 mg/L. A more pronounced decrease in the removal efficiency of SHI-C and SHI-BTCA shives occurred by raising the pollutant concentration from 200 up to 300 mg/L. Nevertheless, the results are interesting because about 70% of the metal present in a solution containing 300 mg Cu/L was eliminated, i.e., an adsorbed quantity of ca. 10 mg per gram of sample.

Another surprising observation was obtained for these two samples at the end of the adsorption process. Indeed, after copper adsorption, the SHI-BTCA shives sample became colored, while those of the SHI-C sample remained colorless (Fig. 2), suggesting different adsorption mechanisms: physisorption (surface adsorption, adsorption onto internal surface and diffusion into cell wall) for SHI-C and chemisorption (complexation, microprecipitation) and ion-exchange for SHI-BTCA [30]. In order to highlight these mechanisms, different microscopic and spectroscopic techniques were performed on the shives samples before and after adsorption (marked as SHI-CCu and SHI-BTCACCu).

Table 1
Characteristics of hemp shives samples.

	SHI-W	SHI-C	SHI-BTCA
Treatment	water washing	Na_2CO_3	grafting
Cellulose	56.93%	62.93%	36.70%
Hemicelluloses	15.42%	9.58%	12.60%
Lignin	26.70%	26.59%	39.60%
Pectins	0.79%	0.42%	3.21%
Fats and waxes	0.39%	0.04%	0.76%
Water solubles	1.11%	0.45%	7.29%
Ion-exchange capacity	0.13 meq/g	0.31 meq/g	1.50 meq/g

3.3. Characterization of the samples before and after copper adsorption

The interactions between copper and hemp-based samples were assessed by using different microscopic and spectroscopic techniques such as computed nano-tomography (nano-CT), energy-disperse X-ray (EDX) spectroscopy, Fourier-transform infrared (FTIR) spectroscopy, Raman spectroscopy, X-ray photoelectron spectroscopy (XPS), and X-ray absorption near-edge structure (XANES) spectroscopy.

Nano-CT images given in Fig. 3a show the typical cross-section of raw hemp shives. Namely, different tissues such as the woody part (xylem) constituting the main part of the shives and some remaining pith on the right side can be observed. The woody part is made of different cell types: i) isolated or grouped in groups of two or three vessels which have a quite thin cell wall and a diameter of approximately 50-150 μm; ii) the fibers with a thick cell wall, an irregular polygonal cross-section and a diameter of only a few μm and iii) the rays which are oriented in the radial direction and are generally composed of one cell in width. The influence of the treatments with Na_2CO_3 and BTCA on the shives SHI-C and SHI-BTCA microstructure is clearly visible on the nano-CT scans (Figs. 3b and 3c, respectively). The removal of a part of the hemicelluloses in the case of sample SHI-C (Table 1) led to the partial deconstruction of the woody fibers cell wall, and general disorganization of the cells within the tissue, which is directly observed through the misorientation and waviness of the woody rays (Fig. 3b). The fiber walls were also strongly affected by grafting (SHI-BTCA), the woody rays degraded, the vessels distorted, and the tissues got fully disorganized as shown in Fig. 3c. The collapse of the fibers was explained by the significant changes in their chemical composition (Table 1). Indeed, the cellulose compartment seems the most affected, with a strong decrease, whereas the lignin content was increased, reflecting an enrichment effect. One can note that the pectin content is also higher in the BTCA sample, suggesting a selective chemical targeting of the treatment on cellulose polymers Fig. 3. also shows EDX spectra of SHI-W, SHI-C, and SHI-BTCA samples before copper adsorption, highlighting the presence of sodium on the surface of hemp shives after Na_2CO_3 treatment and BTCA grafting.

Fig. 4 presents the X-ray nano-CT images and EDX spectra of the raw and modified hemp shives after copper adsorption. No significant effect of the exposition to copper on the shives' microstructure can be detected but a major change in the EDX spectra can be observed. The data point out the presence of peaks that were not observed before the shives immersion in the copper salt solution, which was assigned to copper (see Fig. 4). It is worthy to remind that EDX is a technique for surface characterization with limited penetration in matter thickness. To better identify the spatial localization of the copper in the whole shives' volume, a density-based segmentation of the 3D computed nano-tomography images was done. The obtained images are proposed in Fig. 5. The figures 5 b and d show the typical microstructure of hemp shives where the vessels (v.) are isolated or grouped by two or three, rarely by more, and then they deform one another. The vessels have a quite thin cell wall (p.) and a diameter of approximately 50 to 150 μm (Fig. 5 b). They are surrounded by relatively thick-walled woody fibers (f.) with diameters of only a few μm and an irregularly polygonal section with a rounded cavity. It is evident that copper is adsorbed on all the free

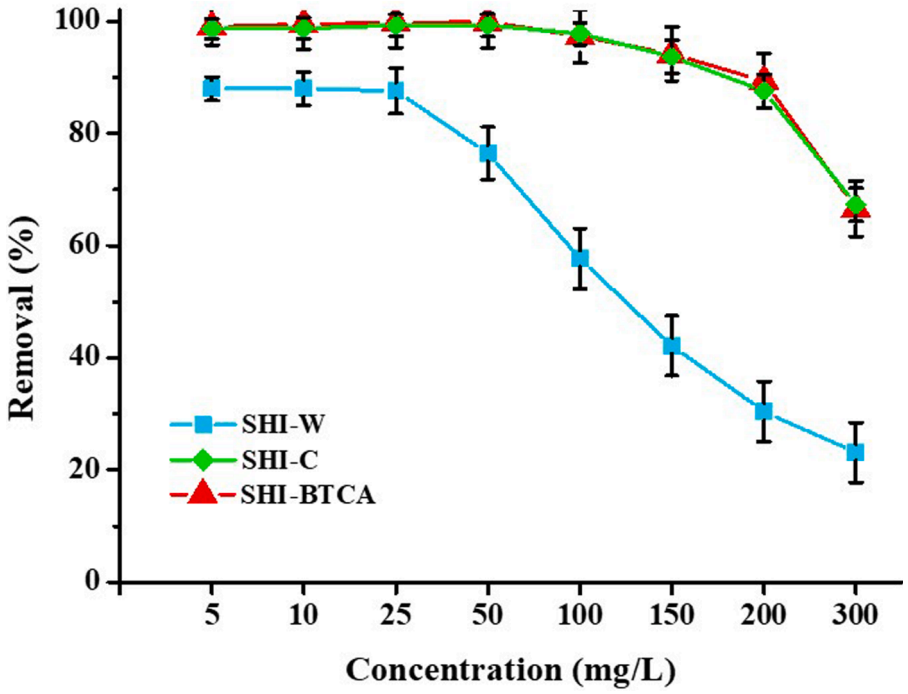

Fig. 1. Effect of initial copper concentration (mg/L) on its removal by three hemp shives samples (adsorbent dose 2 g/100 mL; contact time 120 min; n = 5).

Fig. 2. Hemp shives samples after copper adsorption.

surfaces of the SHI-WCu sample, meaning shives external surface but also on the internal surface of the cells' lumen. The situation is something different in the case of SHI-CCu shives where it is possible to observe that the copper is not only located on the internal surface of the cell wall bordering the lumen but also in the wall itself. This is attributed to the partial removal of the hemicelluloses in the cell wall induced by the treatment with sodium carbonate (Table 1) and by the micro- and nano-porosities created in the cell wall in which the aqueous solution can diffuse. Furthermore, the copper is massively adsorbed on the internal surface of the vessels' wall bordering the lumen of the sample SHI-BTCACu. The BTCA presence allowed more copper to be absorbed in these areas when compared to raw shives, which is in accordance with the results presented in Fig. 1. The detailed analysis of EDX and nano-CT results showed that these two techniques were complementary in revealing the mechanism of copper adsorption on materials. In the EDX spectra (Fig. 4), we can observe an important decrease in the sodium peak and its replacement by copper cations, suggesting the presence of interaction by ion-exchange. In addition, some copper agglomerates (in red color in Fig. 5) are also observed in the internal part of the wall of some of the vessels, suggesting microprecipitation during the adsorption onto the SHI-BTCA sample. So, the results point out that, even if the two treatments (C and BTCA) performed similarly in terms of copper removal, the spatial localization of copper and the adsorption mechanisms were significantly different.

FTIR and Raman spectroscopy were further used for the characterization of the shives before and after copper adsorption (Fig. 6). The main IR and Raman absorption bands and their assignments according to the literature are summarized in Table 2 and Table 3, respectively. These bands were generally attributed to the three main shives components: cellulose, hemicelluloses, and lignin [37–42]. The comparison of SHI-W and SHI-C samples shows an important difference in their IR spectra. Namely, the bands at 1730 cm^{-1} and 1250 cm^{-1} (Fig. 6) assigned to the stretching of unconjugated C=O groups present in hemicelluloses disappeared after the activation with sodium carbonate.

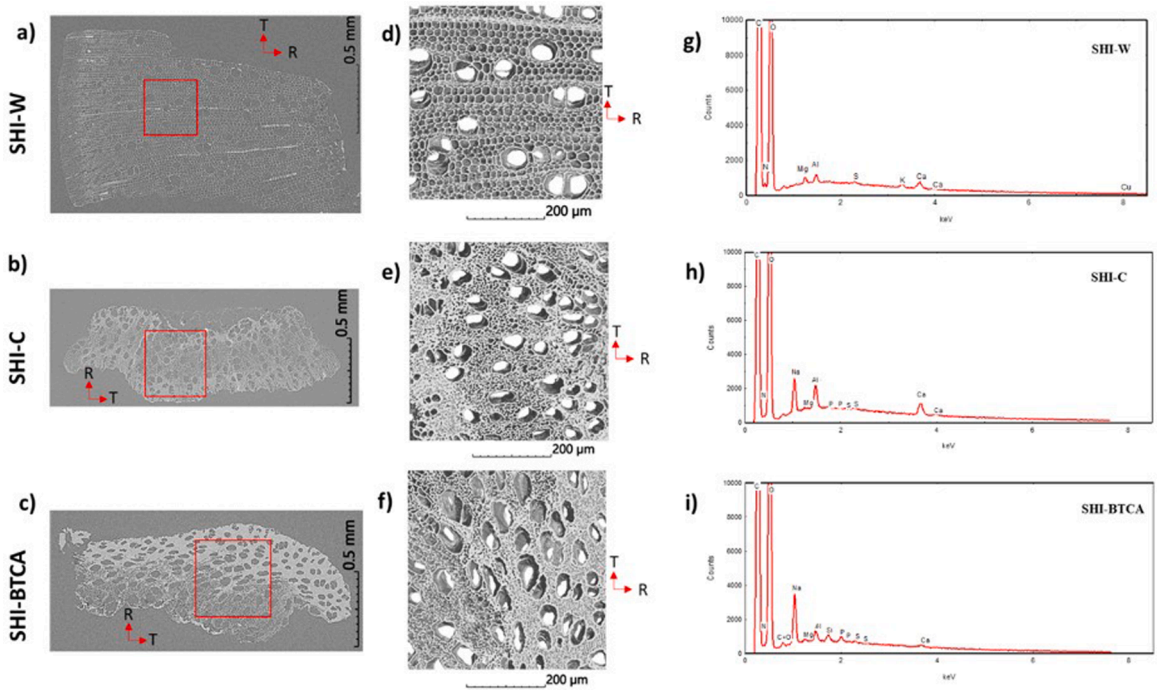

Fig. 3. X-ray nano-tomography images of the transverse cross-sections (left: a, b, and c), computed nano-tomography images (middle: d, e, and f), and EDX spectra (right: g, h, and i) of SHI-W, SHI-C, and SHI-BTCA samples.

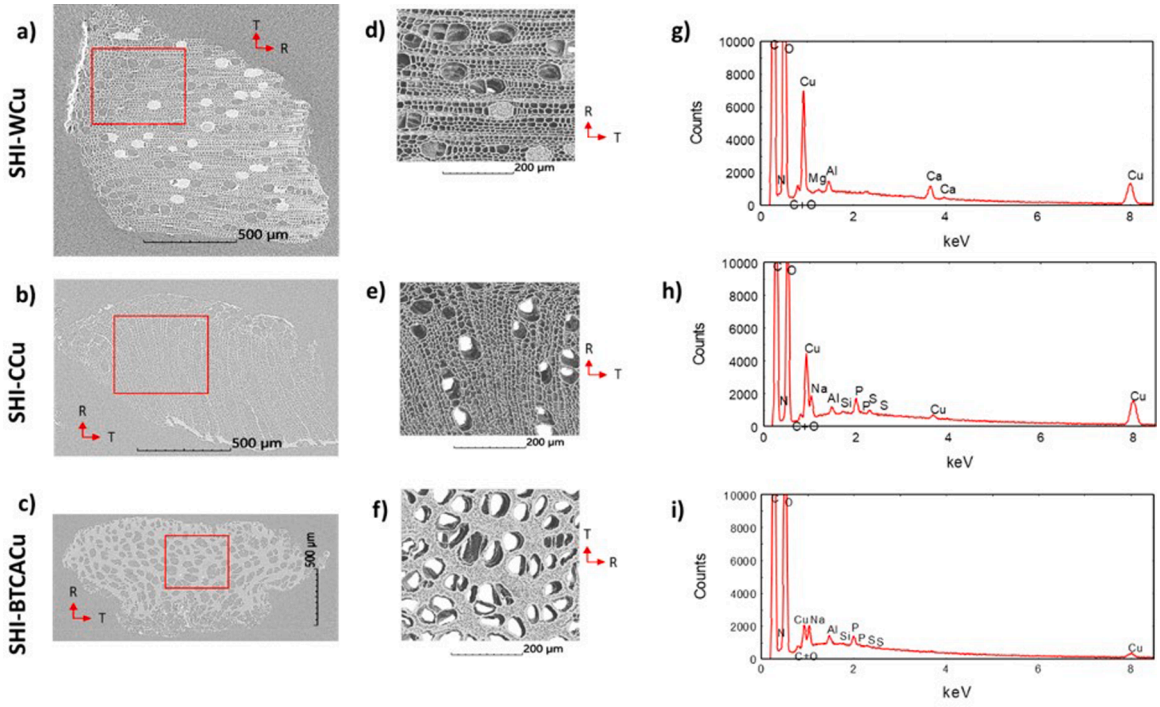

Fig. 4. X-ray nano-tomography images of the transverse cross-sections (left: a, b, and c), computed nano-tomography images (middle: d, e, and f), and EDX spectra (right: g, h, and i) of SHI-WCu, SHI-CCu, and SHI-BTCACu samples after copper adsorption.

This is in agreement with the data of the chemical composition (Table 1) and is also observed after the partial hemicellulose removal from jute fibers using alkaline treatment [43]. When the FTIR spectrum of the SHI-BTCA sample was observed, the bands in the region 1500-1800 cm^{-1} in particular those of the carboxyl (1730 cm^{-1}) and carboxylate (1590 cm^{-1}) groups (Fig. 6), are more intense than in the case of the two other samples which is ascribed to the esterification reaction. In addition, the comparison of SHI-W and SHI-BTCA samples also shows an important increase of the band at 1730 cm^{-1} (due to the BTCA grafting) and a decrease of the band at 1250 cm^{-1} corresponding to the elimination of hemicelluloses enhancing the lignin content in the material.

The interpretation of Raman data indicated that the SHI-W and SHI-C spectra were similar with little differences in the intensity of the bands. On contrary, the Raman spectrum of the SHI-BTCA sample showed an

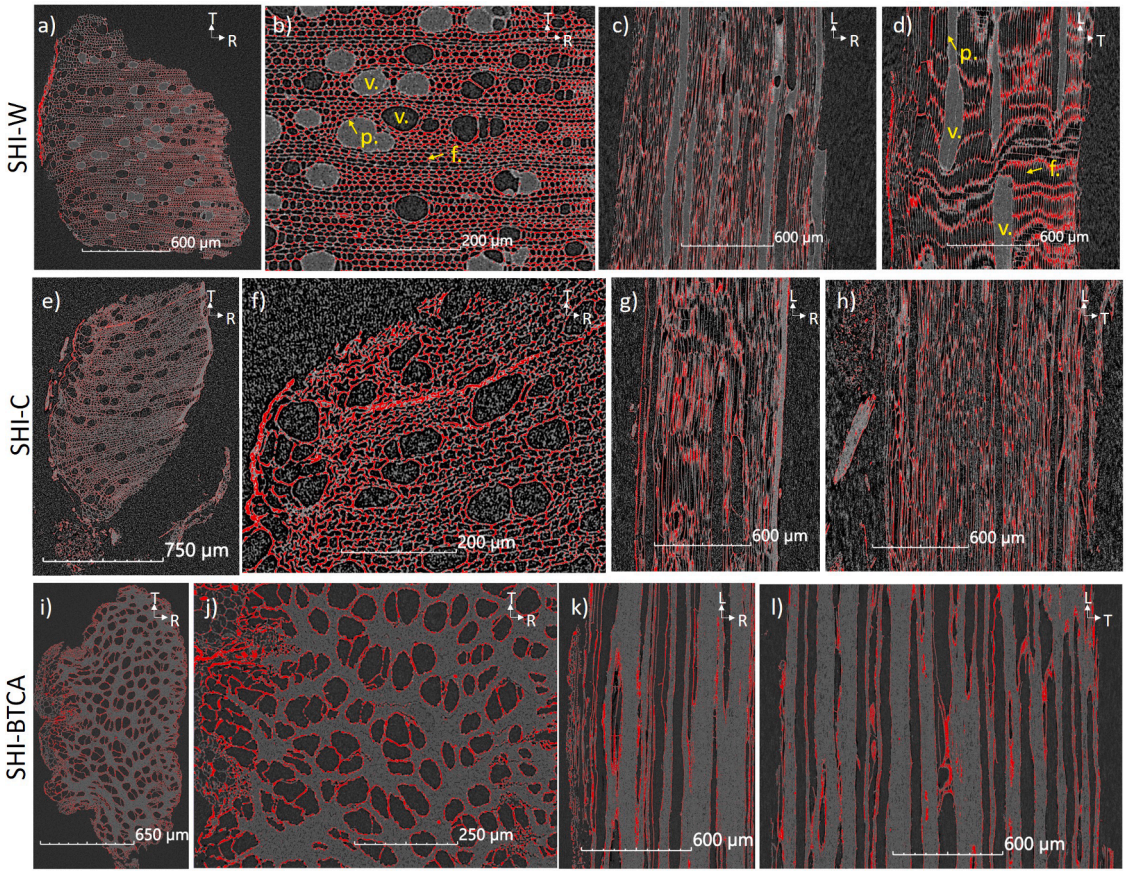

Fig. 5. Density-based segmentation of the X-ray computed nano-tomography images. The high-intensity voxels corresponding to Cu elements are in red color. X-ray nano-tomography images of the different planes are given for SHI-WCu (a-d), SHI-CCu (e-h), and SHI-BTCACu (i-l) specimens (v.: vessel; f.: fiber, p.: pit).

important change in the intensity of the ester band at 1743 cm^{-1}. The comparison between the FTIR and Raman spectra before and after copper adsorption for the studied samples is shown in Fig. 6. After copper adsorption, no changes were observed in the IR spectra of SHI-WCu and SHI-CCu, while the spectrum of SHI-BTCACu showed an important change at 1590 cm^{-1}. Indeed, this band underwent a profound change in both intensity and width, and shifted to 1610 cm^{-1} (Fig. 6). This data reflected the implication of the carboxylate groups on the copper removal through complexation and/or ion-exchange.

By comparing the samples' Raman spectra, we observed that the alkaline activation resulted in the disappearance of the ester band at 1743 cm^{-1}. The addition of copper contributed to obtain samples with a very high sensitivity to burning, resulting in spectra with enhanced background noise. This is the reason why we had to work at 1% laser to avoid such noisy phenomena. However, it was difficult to explain the difference in the ratio between polysaccharides and lignin. In this case, we observed more lignin signals in samples containing copper. SHI-BTCA gave very fluorescent samples, around 60,000 counts in comparison to 10,000 counts or less for SHI-C. For this sample, we also worked with a 1% laser both to avoid the detector's ' saturation and to burn the copper containing sample. The Raman spectrum for SHI-BTCACu also showed the involvement of the ester group in the removal of copper ions, confirming the presence of various interactions between them (chemisorption, ion-exchange). Finally, the Raman spectra of samples after copper adsorption also revealed two bands at 1420 cm^{-1} corresponding to carboxylate group (Fig. 6) and at 885 cm^{-1} (not attributed at the moment), in agreement with IR data.

Fig. 7 compares the XPS wide-spectra of the SHI-W, SHI-C, and SHI-BTCA samples before and after copper adsorption. The spectra obtained before copper adsorption are very similar showing the presence of oxygen (530 eV) and carbon C1s (280 eV) at their surfaces. Nevertheless, the sample SHI-BTCA has an additional peak corresponding to the presence of sodium (Na 1s) localized near the surface at 1072 eV. The presence of this element is due to the conversion of the carboxylic groups into a carboxylate by immersing the BTCA treated shives in a sodium hydrogen carbonate solution. The 1s level of carbon allows access to the different oxygen functions (data not shown). For each sample, C1s can be fitted with four contributions: C–C and C–H bonds at ~284.8 eV (this peak is used for energy calibration and the value of 284.8 eV is fixed), C–OH, and C–O–C bonds at 286.4 eV, O–C–O bonds at around 287.7 eV, and O-C=O for carboxyl groups at about 288.8 eV. The results obtained for SHI-W and SHI-C samples are very similar with a large amount of C-O and C-OH bonds characteristic for cellulose or lignin structure [44,45]. The decomposition of level 1s of carbon is significantly different for sample SHI-BTCA with a strong decrease in C-O / C-OH bonds in favour of carboxylic functions. These results are in agreement with the data of the chemical composition (Table 1). After copper adsorption, Fig. 7 clearly indicates the disappearance of the sodium signal in the SHI-BTCA spectrum, due to the ion-exchange with copper cations.

Fig. 8 shows the main and satellite peaks of Cu $2p_{3/2}$ and Cu $2p_{1/2}$ after copper adsorption onto three studied samples, while Table 4 reports atomic concentrations (in %) of detected elements before and after adsorption. All three samples showed XPS peaks around 933 eV and 953 eV characteristic for Cu $2p_{3/2}$ and Cu $2p_{1/2}$, respectively. The XPS analysis of the Cu 2p peaks showed that this element was not in the same oxidation state in all studied samples (Fig. 8). Indeed, the detection of satellites on the 2p level of copper for the SHI-BTCACu sample makes it possible to deduce also the presence of copper at the oxidation number (+II) for 60%. These satellites are associated with the peak at 934.66 eV

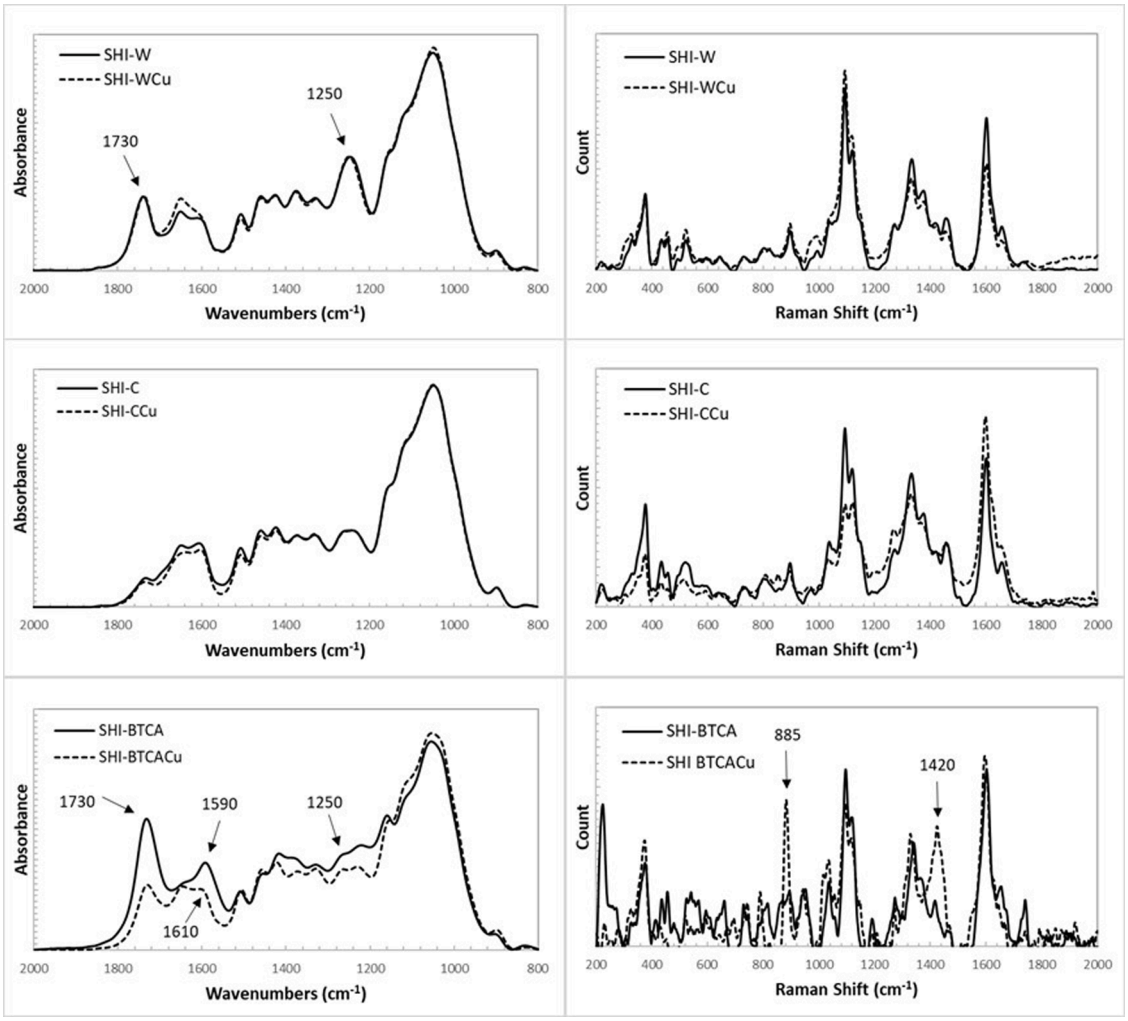

Fig. 6. FTIR (left) and Raman (right) spectra of the SHI-W, SHI-C, and SHI-BTCA samples before and after copper adsorption.

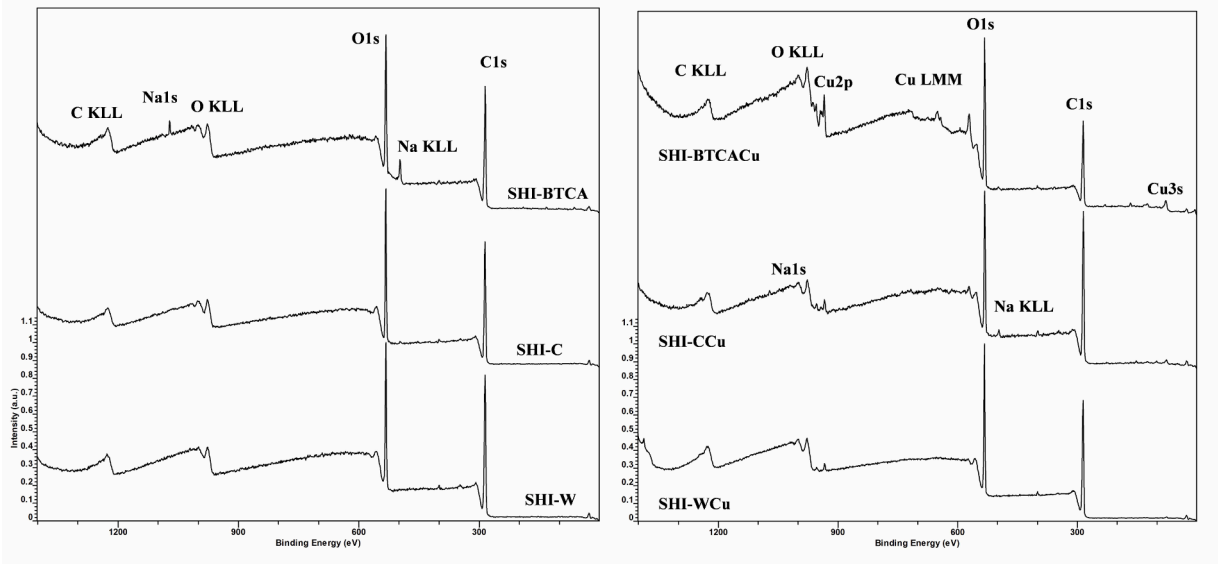

Fig. 7. XPS wide scan spectra of shives before (left) and after (right) copper adsorption.

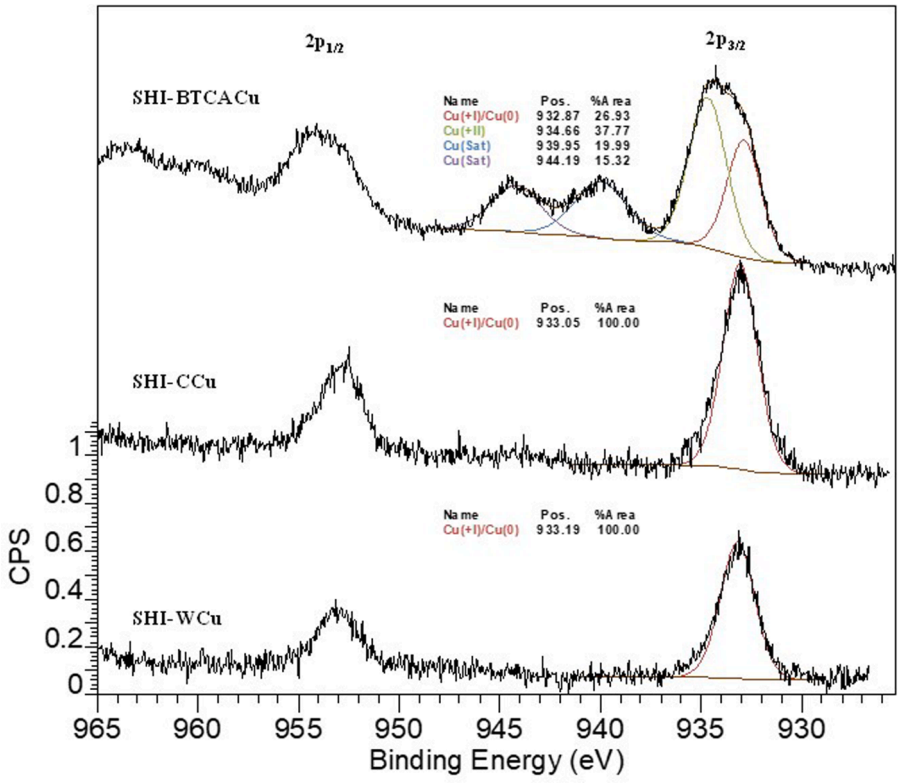

Fig. 8. Main and satellite peaks of Cu $2p_{3/2}$ and Cu $2p_{1/2}$ of the XPS spectra for SHI-WCu, SHI-CCu, and SHI-BTCACu samples after copper adsorption.

of the $2p_{3/2}$ level which corresponds to copper in the form of $Cu(OH)_2$ [33]. In the case of SHI-CCu and SHI-WCu, the detected copper was only in the I oxidation state. Indeed, there are no satellites, the $2p_{3/2}$ level showed only one component at about 933 eV. The measurement of the kinetic energy of the Auger transition of copper $L_3M_{45}M_{45}$ at approximately 913.7 eV allowed us to calculate a modified Auger parameter value at 1846.7 eV close to the species Cu_2O [46]. This shows that the reactions involved in the removal of copper were different for each hemp sample. In order to know the rate of adsorbed copper on the surface, the atomic percentage of copper was calculated from the area of

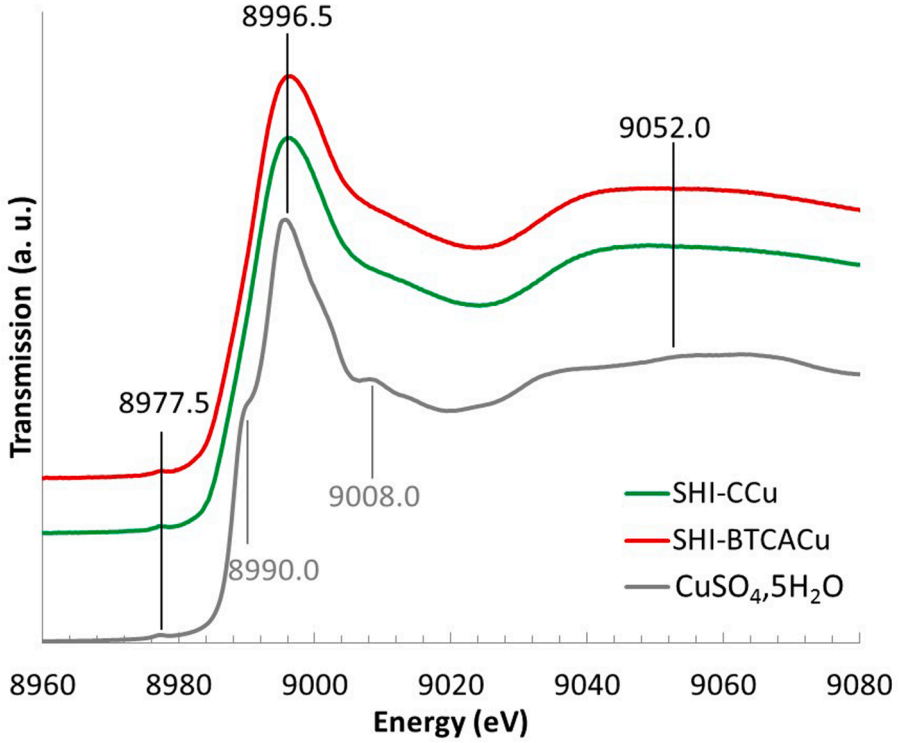

Fig. 9. Cu K-edge XANES spectra of SHI-CCu, SHI-BTCACu, and $CuSO_4,5H_2O$.

the Cu 2p peaks (Table 4). SHI-BTCACu sample had the highest ratio Cu/C = 8.3, followed by SHI-CCu which ratio is 1.5. SHI-WCu sample had a very low Cu/C ratio of 0.4. These results agree with those obtained with other characterization techniques, notably on the fact that copper is well absorbed at the surface for SHI-BTCACu, which gives it this green colour (Fig. 2b). The less important Cu/C ratio for SHI-CCu confirms that, in this case, the mechanism of copper adsorption is different from those of SHI-BTCACu. Namely, the main interaction between copper and sodium carbonate activated shives is diffusion inside the particles.

XANES spectroscopy provides quantitative insight into the oxidation states of copper present in materials [47]. The XANES spectra of SHI-CCu and SHI-BTACCu display the same shape with a pre-edge at 8977.5 eV, the edge at 8991 eV, the maximum of the white line at 8996.5 eV, and a broad oscillation centered on 9052 eV (Fig. 9). The absence of peak around 8983 eV, as found in Cu_2O [48,49], shows that Cu(I) was not detected and that Cu oxidation did not change during the Cu adsorption, it was kept as Cu(II). $CuSO_4{,}5H_2O$ spectrum (Fig. 9) shows specific features such as a shoulder at 8990.0 eV and an oscillation at 9008.0 eV that are not present in hemp samples' spectra. Moreover, the white line of $CuSO_4{,}5H_2O$ spectra is slightly shifted toward lower energies and is more symmetric compared to that in hemp samples' spectra. These differences indicate that after adsorption onto hemp, Cu did not correspond to the crystalline form of $CuSO_4{,}5H_2O$. Furthermore, the hemp samples' spectra are quite different from those of CuO and $Cu(OH)_2$ [48,50], corresponding to other Cu(II)-bearing precipitates. The spectra of hemp samples are similar to the ones of Cu^{2+} measured in liquid phase; $CuSO_4$ [48,51,52] but also $Cu(ClO_4)_2$ [53–55], another Cu complex, both when recorded in a liquid phase.

The results obtained by XANES (only Cu(II)) and those obtained by XPS (only Cu(I) or both Cu(I) and Cu(II)) seems to differ. However, they are compatible and complementary as XANES at Cu K-edge sounded the bulk sample whereas XPS sounded the first atomic layers on the surface of the sample. XANES spectroscopy evidenced that most of the Cu atoms are present in Cu(II) form in both SHI-CCu and SHI-BTCACu samples and XPS spectroscopy indicated that the external surfaces of SHI-WCu and SHI-CCu are coated by Cu_2O and that the external surface of SHI-BTCACu is coated by a mixture of Cu_2O and $Cu(OH)_2$, explaining this characteristic blue color (Fig. 2b).

4. Conclusions

In this work, we have studied the interactions between the copper present in an aqueous solution and hemp-based materials by different microscopic and spectroscopic techniques. The use of EDX, nano-CT, XPS, FTIR, Raman, and XANES spectroscopy permitted to characterize the materials prepared from hemp shives as co-products of the hemp industry (sodium carbonate-activated (SHI-C) and polycarboxylic agent-grafted (SHI-BTCA) hemp shives), before and after copper adsorption, in terms of structure, chemical composition, and chemical state of Cu. The analysis of the data clearly indicated that the adsorption mechanism for copper onto the two materials was different. For SHI-C, surface adsorption and diffusion in the hemp shives structure were suggested, copper diffused into the cell wall. For SHI-BTCA, the adsorption was governed by chemisorption (complexation, microprecipitation) and ion-exchange involving the carboxylate groups in sodium form: copper was preferentially adsorbed on the surface of the inner vessel wall. To continue this work and advance the field, we could be considered to combine X-ray fluorescence mapping with Cu K-edge micro-XANES to focus the analysis on micro-precipitates and the coloration observed for SHI-BTCA after copper adsorption. As suggested by the reviewers, a study will be carried out to determine the thermodynamic properties of the materials to provide information about the inherent energetic changes associated with the adsorption process, e.g., irreversibility and spontaneity of the process, and to confirm the mechanisms using the Gibbs and van't Hoff equations [56–60].

Table 2
The main absorption bands in FTIR spectra of samples and their assignment before copper adsorption (δ: bending vibration; ν: stretching vibration; oop: out of plane).

Wavenumbers (cm^{-1})	Chemical group	Component
1730	C=O ester, COOH	hemicelluloses, pectins, fatty acids, BTCA
1640/1650	δ (OH) adsorbed water, ν (C=O, N-H)	water, proteins, cellulose, lignin
1600	ν (C=C aromatic)	lignin, phenolics
1590	COO^-	BTCA
1550	ν (C-N), δ (N-H)	proteins
1515	ν (C=C aromatic)	lignin, phenolics
1460	ν (C=C aromatic)	lignin
1430	δ (CH_2), ν_{as} (CH_3)	cellulose
1420	ν (C=C aromatic)	lignin, phenolics
1375	δ (CH_2)	cellulose, hemicelluloses
1250	δ (CH), δ (OH) O-acetyl	hemicelluloses
1215	δ (CH), δ(OH)	cellulose, hemicelluloses
1165	ν (C-O-C)	cellulose, hemicelluloses
1110	ν (CC, CO)	cellulose, hemicelluloses
1060	ν (CC, CO)	cellulose
1040	ν (CC, CO), δ(COH)	hemicelluloses
1030	ν (CC, CO)	cellulose
895	β (1-4) glycoside	cellulose
815	δ (CH) oop	lignin, phenolics

Table 3
The main absorption bands in Raman spectra of samples and their assignment before copper adsorption.

Wavenumbers (cm^{-1})	Chemical group	Component
1743	C=O ester	lignin
1660	ν (C=O)	proteins
1605	COO^-	acid
1600	ν (C=C aromatic)	lignin
1460	δ (O-CH_3), δ (C-H_2)	cellulose, hemicelluloses, lignin
1420	δ (HC-C, HC- O), COO^-, δ (C-$H)_3$	hemicelluloses, lignin
1380	δ (HC-C), δ (HC-O), δ C-OH)	cellulose, hemicelluloses
1337	δ (CH), δ (COH)	cellulose, lignin
1284	δ (=C-H ip)	phenolic acid
1120	ν (C-C, HC-O, ν_{as} (C-O-C)	cellulose, hemicelluloses
1095	ν (C-C, HC-O, ν_s (C-O-C)	cellulose, hemicelluloses
1040	ν (CC, CO), δ (COH)	hemicelluloses
895	β (1-4) glycoside	cellulose
885	-	-
380	δ skeletal mode	Iβ cellulose

Table 4
Atomic concentrations (%) of detected elements before and after copper adsorption determined from XPS spectra (n.d.: not detected).

	Carbon	Copper	% (Cu/C)	Sodium	Oxygen
SHI-W	73.3	n.d.	n.d.	0.1	26.6
SHI-WCu	69.4	0.3	0.4	n.d.	30.2
SHI-C	69.7	n.d.	n.d.	0.2	30.1
SHI-CCu	72.0	1.1	1.5	0.4	26.5
SHI-BTCA	68.8	n.d.	n.d.	1.5	29.7
SHI-BTCACu	59.0	4.9	8.3	0.7	35.5

Declaration of Competing Interest

The authors declare that they have no known competing financial interests or personal relationships that could have appeared to influence the work reported in this paper. They have read and agreed to the published version of the article.

Acknowledgments

G.C. and N.M.C thank the Région Bourgogne Franche-Comté (France), FEDER (Fonds Européen de Développement Régional), Silac Industrie (Champlitte, France) and Eurochanvre (Arc-les-Gray, France) for financial support (FINEAU Program 2021-2024: an European project focused on "Plant-Based Cellulosic Materials for Wastewater Treatment"). The doctoral student Chiara Mongioví thanks the Région Bourgogne Franche-Comté (France) for awarding her a research grant. This work has also been supported by the EIPHI Graduate school (contract "ANR-17-EURE-0002"). The authors are grateful to the PEA^{2}t (Chrono-environnement, France), MIFHySTO (FEMTO-ST, France), MIMENTO (French RENATECH network), and SAMBA Beamline (SOLEIL Synchrotron France, experiment on in-house beamtime) platforms which manage and maintain the analytical equipment used in this study. A.R.L.R. would like to thank FCT funding under the DL57/2016 Transitory Norm Programme and the scientific collaboration under project Base-UIDB/50020/2020 and Programmatic-UIDP/50020/2020 funding of LSRE-LCM, funded by national funds through FCT/MCTES (PIDDAC). Finally, the authors would also like to thank the anonymous reviewers: we appreciated all their constructive comments and suggestions for improving the paper.

References

[1] P. Bouloc, Hemp: industrial production and uses, CABI, Oxfordshire (2013) 312.
[2] K. Żuk-Gołaszewska, J. Gołaszewski, Cannabis sativa L. - Cultivation and quality or raw material, J. Elem. 23 (2018) 971–984.
[3] M. Kostić, M. Vukčević, B. Pejić, A. Kalijadis, Hemp fibers: old fibers - new applications. In: Textiles: History, Properties and Performance and Applications, Ibrahim Md, Mondal M, (eds). Nova Science Publishers, New York, Inc., 2014, pp 399-446.
[4] M. Kostić, B. Pejić, M. Vukčević, Cellulose provenant de fibres libériennes et autres fibres textiles - nouvelles applications. In: chimie pour la transformation durable de la ressource lignocellulosique, In: Stevanovic T (ed). Bordo: Presses Universitaires, Bordeaux, 2019, pp 27-69.
[5] N.T. Dunford, Hemp and flaxseed oil: properties and applications for use in food, In: specialty oils and fats in food and nutrition: properties, processing and applications. Talbot G (ed), Elsevier, 2015, pp 39-63.
[6] C. Ingrao, A. Lo Giudice, J. Bacenetti, C. Tricase, G. Dotelli, M. Fiala, V. Siracusa, C. Mbohwa, Energy and environmental assessment of industrial hemp for building applications: a review, Renew. Sust. Energ. Rev. 51 (2015) 29–42.
[7] J.H. Cherney, E. Small, Industrial hemp in North America: production, politics and potential, Agronomy 6 (2016) 1–24.
[8] J. Fike, Industrial hemp: renewed opportunities for an ancient crop, Critical Rev. Plant. Sci. 35 (2016) 406–424.
[9] G. Crini, E. Lichtfouse, Green adsorbents for pollutant removal. Fundamentals and design, Environmental Chemistry for a sustainable World. Springer Nature Switzerland, 2019.
[10] G. Crini, E. Lichtfouse, Hemp production and applications, Sustainable Agriculture Reviews 42. Springer Nature Switzerland, Cham, 2020.
[11] G. Crini, E. Lichtfouse, G. Chanet, N. Morin-Crini, Applications of hemp in textiles, paper industry, insulation and building materials, horticulture, animal nutrition, food and beverages, nutraceuticals, cosmetics and hygiene, medicine, agrochemistry, energy production and environment, Environ. Chem. Lett. 18 (2020) 1451–1476.
[12] E. Terpáková, L. Kidalová, A. Eštoková, J. Čigášová, N. Števulová, Chemical modification of hemp shives and their characterization, Procedia Eng 42 (2012) 931–941.
[13] N. Števulová, J. Čigášová, A. Eštoková, E. Terpáková, A. Geffert, F. Kacik, E. Singovska, M. Holub, Properties characterization of chemically modified hemp hurds, Materials 7 (2014) 8131–8150.
[14] C. Păduraru, L. Tofan, Investigations on the possibility of natural hemp fibers use for Zn(II) removal from wastewaters, Environ. Eng. Manage. J. 7 (2008) 687–693.
[15] I. Rezić, Cellulosic fibers - Biosorptive materials and indicators of heavy metal pollution, Microchem. J. 107 (2013) 63–69.
[16] M. Balintova, M. Holub, N. Števulová, J. Čigášová, M. Tesarcikova, Sorption in acidic environment - Biosorbents in comparison with commercial adsorbents, Chem. Eng. Trans. 39 (2014) 625–630.
[17] G.Z. Kyzas, M. Kostoglou, Green adsorbents for wastewaters: a critical review, Materials 7 (2014) 333–364.
[18] J. Bugnet, N. Morin-Crini, C. Cosentino, G. Chanet, P. Winterton, G. Crini, Hemp decontamination of poly-metallic aqueous solutions, Environ. Eng. Manage. J. 16 (2017) 535–542.
[19] L. Rozumová, B. Legátová, J. Prehradná, Potential of the biosorbents from waste for the separation of Cu(II) from aqueous solutions, Key Eng. Mater. 779 (2018) 102–109.
[20] L. Rozumová, B. Legátová, Biosorbent from industrial hemp hurds for copper ions removal, Int. J. Mater. Sci. Eng. 6 (2018) 114–125.
[21] N. Morin-Crini, S. Loiacono, V. Placet, G. Torri, C. Bradu, M. Kostić, C. Cosentino, G. Chanet, B. Martel, E. Lichtfouse, G. Crini, Hemp-based adsorbents for sequestration of metals, Environ. Chem. Lett. 17 (2019) 393–408.
[22] L. Tofan, C. Păduraru, C. Teodosiu, Hemp fibers for wastewater treatment, Hemp production and applications, Crini G, Lichtfouse E (eds), Sustainable Agriculture Reviews 42 (2020) 295–326.
[23] Z. Bai, Q. Liu, H. Zhang, J. Liu, J. Yu, J. Wang, A novel 3D reticular anti-fouling bio-adsorbent for uranium extraction from seawater: Polyethylenimine and guanidyl functionalized hemp fibers, Chem. Eng. J. 382 (2020), 122555.
[24] M. Vukčević, B. Pejić, A. Kalijadis, I. Pajić-Lijaković, M. Kostić, Z. Laušević, M. Laušević, Carbon materials from waste short hemp fibers as a sorbent for heavy metal ions - Mathematical modeling of sorbent structure and ions transport, Chem. Eng. J. 235 (2014) 284–292.
[25] G. Crini, C. Bradu, C. Cosentino, J.N. Staelens, B. Martel, M. Fourmentin, S. Loiacono, G. Chanet, G. Torri, N. Morin-Crini, Simultaneous removal of inorganic and organic pollutants from polycontaminated wastewaters on modified hemp-based felts, Rev. de Chim. 72 (2021) 25–43.
[26] M.M. Vukčević, B.M. Pejić, I.S. Pajić-Lijaković, A.M. Kalijadis, M.M. Kostić, Z. V. Laušević, M.D. Laušević, Influence of the precursor chemical composition on heavy metal adsorption properties of hemp (*Cannabis sativa*) fibers based biocarbon, J. Serb. Chem. 82 (2017) 1417–1431.
[27] M. Dizbay-Onat, U.K. Vaidya, J.A.G. Balanay, C.T. Lungu, Preparation and characterization of flax, hemp and sisal fiber-derived mesoporous activated carbon adsorbents, Adsorption Sci. Technol. 36 (2018) 441–457.
[28] B. Doczekalska, K. Kusmierek, A. Swiatkowski, M. Bartkowiak, Adsorption of 2,4-dichlorophenoxyacetic acid and 4-chloro-2-metylphenoxyacetic acid onto activated carbons derived from various lignocellulosic materials, J. Environ. Sci. Health. 53 (2018) 290–297.
[29] Y. Jiang, M.P. Ansell, X. Jia, A. Hussain, M. Lawrence, Physical characterization of hemp shiv: Cell wall structure and porosity, Academic J. Civil Eng. 35 (2017) 22–28.
[30] C. Mongioví, D. Lacalamita, N. Morin-Crini, X. Gabrion, V. Placet, A.R.L. Ribeiro, A. Ivanovska, M. Kostić, C. Bradu, G. Crini, Use of chènevotte, a valuable co-product of industrial hemp fiber, as adsorbent for pollutant removal: Kinetic studies and modeling, Arabian J. Chem. 15 (2022), 103742.
[31] C. Mongioví, D. Lacalamita, N. Morin-Crini, X. Gabrion, A. Ivanovska, F. Sala, V. Placet, V. Rizzi, J. Gubitosa, E. Mesto, A.R.L. Ribeiro, P. Fini, N. De Vietro, E. Schingaro, M. Kostić, C. Cosentino, P. Cosma, C. Bradu, G. Chanet, G. Crini, Use of chènevotte, a valuable co-product of industrial hemp fiber, as adsorbent for pollutant removal. Part I. Chemical, microscopic, spectroscopic and thermogravimetric characterization of raw and modified samples, Molecules 26 (2021) 4574.
[32] S. Loiacono, G. Crini, B. Martel, G. Chanet, C. Cosentino, M. Raschetti, V. Placet, G. Torri, N. Morin-Crini, Simultaneous removal of Cd, Co, Cu, Mn, Ni, and Zn from synthetic solutions on a hemp-based felt. II. Chemical modification, J. Appl. Polym. Sci 134 (2017) 45138.
[33] M.C. Biesinger, Advanced analysis of copper X-ray photoelectron spectra, Surf. Int. Anal. 49 (2017) 1325–1334.
[34] N. Fairley, V. Fernandez, M. Richard-Plouet, C. Guillot-Deudon, J. Walton, E. Smith, D. Flahaut, M. Greiner, M. Biesinger, S. Tougaard, D. Morgan, J. Baltrusaitis, Systematic and collaborative approach to problem solving using X-Ray photoelectron spectroscopy, Appl. Surf. Sci. 5 (2021), 100112.
[35] B. Ravel, M. Newville, ARTEMIS ATHENA, HEPHAESTUS: data analysis for X-ray absorption spectroscopy using IFEFFIT, J. Synchrotron Radiat. 12 (2005) 537–541.
[36] A. Ivanovska, J. Lađarević, L. Pavun, B. Dojčinović, I. Cvijetić, D. Mijin, M. Kostić, Obtaining jute fabrics with enhanced sorption properties and "closing the loop" of their lifecycle, Ind. Crops. Products. 171 (2021), 113913.
[37] J.H. Wiley, R.H. Atalla, Band assignments in the Raman spectra of celluloses, Carbohydr. Res. 160 (1987) 113–129.
[38] M. Kačuráková, N. Wellner, A. Ebringerová, Z. Hromádková, R.H. Wilson, P. S. Belton, Characterisation of xylan-type and associated cell wall components by FT-IR and FT-Raman spectroscopies,, Food Hydrocoll. 13 (1999) 35–41.
[39] H. Schulz, M. Baranska, Identification and quantification of valuable plant substances by IR and Raman spectroscopy, Vib. Spectrosc. 43 (2007) 13–25.
[40] U.P. Agarwal, J.D. McSweeny, S.A. Ralph, FT-Raman investigation of milled-wood lignins: Softwood, hardwood, and chemically modified black spruce lignins, J. Wood Chem. Technol. 31 (2011) 324–344.
[41] X.J. Fu, G. Yang, J.B. Sun, J. Zhou, Vibrational spectra of copper sulfate hydrates investigated with low-temperature Raman spectroscopy and terahertz time domain spectroscopy, J. Phys. Chem. A. 116 (2012) 7314–7318.
[42] R. Chazal, P. Robert, S. Durand, M.F. Devaux, L. Saulnier, C. Lapierre, F. Guillon, Investigating lignin key features in maize lignocelluloses using infrared spectroscopy, Appl. Spectro. 68 (2014) 1342–1347.
[43] A. Ivanovska, K. Asanovic, M. Jankoska, K. Mihajlovski, L. Pavun, M Kostić M, Multifunctional jute fabrics obtained by different chemical modifications, Cellulose 27 (2020) 8485–8502.
[44] K.M. Vanhatalo, N. Maximova, A.M. Perander, L.S. Johansson, E. Haimi, O. Dahl, Comparison of conventional and lignin-rich microcrystalline cellulose, Bioresources 11 (2016) 4037–4054.
[45] T. Eleutério, S. Sério, O.M.N.D. Teodoro, N. Bundaleski, H.C. Vaconcelos, XPS and FTIR studies of DC reactive magnetron sputtered TiO_2 thin films on natural based-cellulose fibers, Coatings 10 (2020) 284.

[46] M.C. Biesinger, L.W.M. Lau, A.R. Gerson, R.S.C. Smart, Resolving surface chemical states in XPS analysis of first row transition metals, oxides and hydroxides: Sc, Ti, V, Cu and Zn, Appl. Surf. Sci. 257 (2010) 887–898.
[47] M.A. Newton, A.J. Knorpp, A.B. Pinar, V.L. Sushkevich, D. Palagin, J.A. van Bokhoven, On the mechanism underlying the direct conversion of methane to methanol by copper hosted in zeolites; Braiding Cu K-edge XANES and reactivity studies, J. Am. Chem. Soc. 140 (2018) 10090–10093.
[48] M. Larsson, J.B. Lindén, S. Kaur, B.Le Cerf, I. Kempson, Cu K-edge XANES: polymer, organic, inorganic spectra, and experimental considerations, Powder Diffr. 32 (2017). S28-S32.
[49] M. Ferrandon, V.N. Daggupati, Z. Wang, G. Naterer, G.N. Trevani, Using XANES to obtain mechanistic information for the hydrolysis of $CuCl_2$ and the decomposition of Cu_2OCl_2 in the thermochemical Cu-Cl cycle for H_2 production, J. Therm. Anal. Calorim. 119 (2014) 975–982.
[50] Z.G. Qin, Q.J. Xiang, F. Liu, J. Xiong, L.K. Koopal, L.R. Zheng, M. Ginder-Vogel, M. X. Wang, X.H. Feng, W.F. Tan, H. Yin, Local structure of Cu^{2+} in Cu-doped hexagonal turbostratic birnessite and Cu^{2+} stability under acid treatment, Chem. Geol 466 (2017) 512–523.
[51] S.W.T. Price, J.D. Speed, P. Kannan, A.E. Russell, Exploring the first steps in core-shell electrocatalyst preparation: In situ characterization of the under potential deposition of Cu on supported Au nanoparticles, J. Am. Chem. Soc. 133 (2011) 19448–19458.
[52] P. Unwiset, A. Makdee, K.C. Chanapattharapol, P. Kidkhunthod, Effect of Cu addition on TiO2 surface properties and photocatalytic performance: X-ray absorption spectroscopy analysis, J. Phys. Chem. Solids. 120 (2018) 231–240.
[53] D. Bowron, M. Amboage, R. Boada, A. Freeman, S. Hayama, S. Díaz-Moreno, The hydration structure of Cu^{2+}: More tetrahedral than octahedral? RSC Adv 3 (2013) 17803–17812.
[54] P. Frank, M. Benfatto, M. Qayyam, B. Hedman, K.O. Hodgson, A high-resolution XAS study of aqueous Cu(II) in liquid and frozen solutions: Pyramidal, polymorphic, and non-centrosymmetric, J. Chem. Phys. 142 (2015), 084310.
[55] P. Frank, M. Benfatto, M. Qayyum, $[Cu(aq)]^{2+}$ is structurally plastic and the axially elongated octahedron goes missing, J. Chem. Phys. 148 (2018), 204302.
[56] N. Yao, X. Zhang, Z. Yang, W. Yang, Z. Tian, L. Zhang, Norfloxacin and bisphenol-A removal using temperature-switchable graphene oxide, ACS Appl. Mater. Interfaces 10 (2018) 29083–29091.
[57] X. Zhang, J. Shen, N. Zhuo, Z. Tian, P. Xu, Z. Yang, W. Yang, Interactions between antibiotics and graphene-based materials in Water: A comparative experimental and theoretical investigation, ACS Appl. Mater. Interfaces 8 (2016) 24273–24280.
[58] M. González-López, C.M. Laureano-Anzaldo, A.A. Pérez-Fonseca, M. Arellano, J. R. Robledo-Ortíz, A critical overview of adsorption models linearization: Methodological and statistical inconsistencies, Sep. Purif. Rev. (2021), https://doi.org/10.1080/15422119.2021.1951757.
[59] M.I.A.A. Maksoud, A.M. Elgarahy, C. Farrell, A.H. Al-Muhtaseb, D.W. Rooney, A. I. Osman, Insight on water remediation application using magnetic nanomaterials and biosorbents, Coord. Chem. Rev 403 (2020), 213096.
[60] L. Alcaraz, I. García-Díaz; F. J. Alguacil, F. A. López, Removal of copper ions from wastewater by adsorption onto a green adsorbent from winemaking wastes, 15 (2020) 1112-1133.